

# Injection Locking of Linearlike and Soliton Spin-Wave Modes in Nanoconstriction Spin Hall Nano-oscillators

Mona Rajabali<sup>1,\*</sup>, Roman Ovcharov<sup>1</sup>, Roman Khymyn<sup>1</sup>, Himanshu Fulara<sup>2</sup>, Akash Kumar<sup>1</sup>, Artem Litvinenko<sup>1</sup>, Mohammad Zahedinejad<sup>1</sup>, Afshin Houshang<sup>1</sup>, Ahmad A. Awad<sup>1,3,4</sup>, and Johan Åkerman<sup>1,3,4,†</sup>

<sup>1</sup>Department of Physics, University of Gothenburg, Gothenburg 412 96, Sweden

<sup>2</sup>Department of Physics, Indian Institute of Technology Roorkee, Roorkee 247667, India

<sup>3</sup>Research Institute of Electrical Communication, Tohoku University, 2-1-1 Katahira, Aoba-ku, Sendai 980-8577, Japan

<sup>4</sup>Center for Science and Innovation in Spintronics, Tohoku University, 2-1-1 Katahira, Aoba-ku, Sendai 980-8577, Japan

(Received 5 August 2022; revised 21 November 2022; accepted 1 February 2023; published 22 March 2023)

We study injection locking of two different spin wave (SW) modes (a field-localized linearlike interior mode and a self-localized SW bullet soliton) in a single nanoconstriction-based spin Hall nano-oscillator. Mode selection is achieved by varying the oblique magnetic field angle and magnitude. The two modes show dramatically different responses to injection locking, in terms of locking bandwidth and linewidth and output power in the locked state. Extracting the locking range graphically from the experimental data yields apparent thresholds for the required injected power, with the bullet mode showing a larger threshold than the linearlike mode. By instead fitting the full detuning behavior using a model including thermal noise, the apparent threshold vanishes, while the very different locking behavior of the two modes can instead be ascribed to the order of magnitude difference in their mode volumes.

DOI: 10.1103/PhysRevApplied.19.034070

## I. INTRODUCTION

Injection locking is a fundamental nonlinear phenomenon in which an external signal enforces its frequency onto an otherwise free-running auto-oscillator [1]. In spintronics, both spin torque and spin Hall nano-oscillators [2] (STNOs and SHNOs) can be readily injection-locked, via either a microwave current [3–12] or a microwave field [13–18]. Injection locking of such oscillators has recently been used for various communication schemes, such as phase-shift keying [19,20], and emerging computation schemes, such as neuromorphic computing [21–26]. SHNOs based on nanoconstrictions (NCs) [27] have shown particular potential as they can be mutually synchronized in long chains [28,29] and two-dimensional arrays [23]. Due to their simple bilayer structure, they offer straightforward fabrication, flexibility in material choices,

freedom in device layout, and direct optical access to the active auto-oscillating region. SHNOs also exhibit a robust frequency response [30], wide frequency tunability [31], and fast modulation rates [32], as well as easy injection locking [12]. However, so far, no studies have looked into the details of how the different spin wave (SW) modes in NC-SHNOs injection-lock to microwave currents.

In contrast to STNO injection locking, studies on nanogap SHNOs [33] demonstrated the existence of a significant threshold in the external microwave power required for successful injection locking. The threshold was ascribed to the nonlinear self-localized nature of the auto-oscillating SW bullet mode [34,35]. As NC-SHNOs can sustain a wide range of qualitatively different SW modes (field-localized edge modes [27,28,36], self-localized edge bullets [36–38], field-localized internal constriction modes [28,36], full constriction modes [39], magnetic droplets [40], and propagating SWs [41,42]), one would expect the injection-locking behavior to be very rich. Depending on field conditions, one should also be able to use the same device to study how different modes respond to injection locking.

Here we carry out a detailed injection-locking study of NC-SHNOs when subjected to an injection locking at twice their frequency. We can drive distinctly different

\*mona.rajabali@gmail.com

†johan.akerman@physics.gu.se

Published by the American Physical Society under the terms of the [Creative Commons Attribution 4.0 International license](#). Further distribution of this work must maintain attribution to the author(s) and the published article's title, journal citation, and DOI. Funded by [Bibsam](#).

SW modes merely by changing the external field conditions. We focus on two very different modes—a linearlike interior SW mode, and a self-localized SW (edge) bullet—which show dramatically different injection locking. Their respective response is, in fact, so different that it is, at first, not obvious how to find a common definition for extracting the locking range from experimental data. We try different approaches to defining the locking range and find that they reproduce an apparent large threshold for injection locking of the soliton mode [33]. However, by applying a model based on the theory [43] for auto-oscillator injection locking in the presence of noise, we find that the very different locking behaviors of the two modes originate from the one-order-of-magnitude difference in their intrinsic noise levels; their *intrinsic* locking bandwidths are otherwise similar. The presence of thermal noise can hence manifest itself in an apparent threshold for injection locking of small volume modes, such as the bullet, while larger-volume modes are less impacted. While it is straightforward to analyze injection locking of nonlinear oscillators with low intrinsic noise, our work highlights that a more complete model, where noise is directly included, should be used for low-volume modes, in particular for the SW bullet investigated in this work.

## II. EXPERIMENTAL PART

NC-SHNOs were fabricated from heterostructures of Py(5nm)(Ni<sub>80</sub>Fe<sub>20</sub>)/Pt(5nm)/AlO<sub>x</sub>(2nm). The stack was magnetron-sputtered at room temperature onto a 20 × 20 mm<sup>2</sup> piece of *c*-plane sapphire substrate in a system with a base pressure lower than 3 × 10<sup>-8</sup> torr. The stack was then patterned into 4 × 12 μm<sup>2</sup> rectangles with bowtie-shaped NCs, using a Raith EBPG 5200 100-keV EBL system and an Oxford Dry etch 400 Plus Ar-ion beam etching (IBE). Finally, optical lithography was carried out to define a coplanar waveguide (CPW), followed by a deposition and liftoff process where a bilayer of Cu(500 nm)/Pt(20 nm) is utilized as top contacts.

A schematic of the SHNO and details of the layer thicknesses are shown in Fig. 1(a), where the inset is a top-view scanning electron microscopy (SEM) image of a 120-nm-wide SHNO. Electrical microwave measurements were done using a custom-built setup in which an out-of-plane magnetic field, specified in Fig. 1(a), was applied to the sample and a direct current drives the auto-oscillations. A microwave current was injected through a circulator to perform the injection locking, where the resulting auto-oscillating signal is in turn amplified and recorded by a spectrum analyzer [Fig. 1(b)].

## III. RESULTS AND DISCUSSION

Figure 2(a) shows the power spectral density (PSD) versus drive current ( $I_{DC}$ ) for a free-running 120-nm-wide SHNO in two qualitatively different operating regimes. In

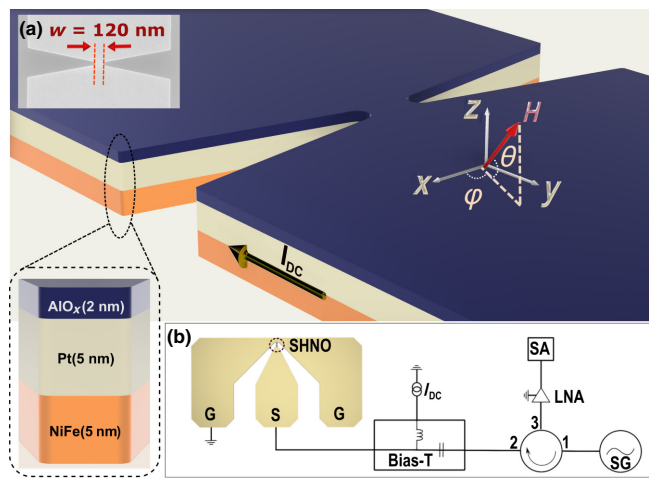


FIG. 1. (a) Device schematic and applied field direction in combination with the device layer structure Py/Pt/AlO<sub>x</sub>, in the lower inset. The inset in the upper left corner shows a top-view SEM image of the SHNO, where  $w$  is the width of the constriction. (b) Schematic of the injection-locking measurement circuit.

Fig. 2(a), both the magnetic field strength (680 mT) and angle ( $\theta = 80^\circ$ ) are high enough to pull the magnetization into a sufficiently out-of-plane angle and suppress the formation of an SW bullet soliton [35,36]. The frequency shows the typical nonmonotonic current dependence as the auto-oscillations start at the NC edge at a low current and then move inwards into the interior of the NC as the current increases [36]; henceforth, we call this mode the interior mode.

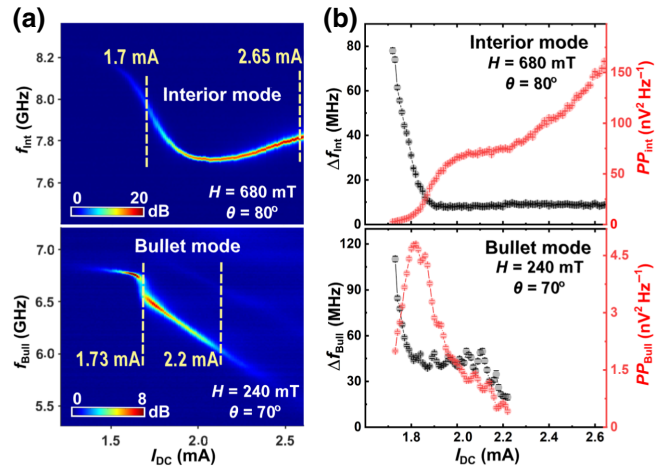


FIG. 2. (a) Power spectral density versus drive current of an NC-SHNO with  $w = 120$  nm under two different field conditions: a 680-mT field applied at an oblique angle  $\theta = 80^\circ$  and an in-plane angle  $\varphi = 22^\circ$  (top); and a 240-mT field applied at  $\theta = 70^\circ$  and  $\varphi = 22^\circ$  (bottom). (b) The extracted linewidth and peak power for interior (top) and bullet (bottom) modes, obtained by analyzing PSDs in (a).

When the field strength and  $\theta$  are reduced to 240 mT and  $70^\circ$ , respectively, the mode transitions into a self-localized SW bullet located at one of the constriction edges. By changing the field conditions, we can hence realize these distinctly different auto-oscillating SW modes and study their injection-locking behavior in the same device. In the following, we label all measured and extracted microwave signal properties of these two modes with Int (interior) and Bull (bullet).

As can be seen in Fig. 2(b), where we plot the extracted linewidth ( $\Delta f$ ) and peak power ( $PP$ ), the two modes differ dramatically in their microwave signal properties. With increasing  $I_{DC}$ ,  $\Delta f_{\text{Int}}$  rapidly drops and reaches below the resolution bandwidth (RBW; 10 MHz) used in the measurement. The linewidth of the bullet mode ( $\Delta f_{\text{Bull}}$ ), on the other hand, first stabilizes around 40–50 MHz before slightly improving just before its signal disappears below the noise floor at  $I_{DC} = 2.2$  mA. The peak power is also very different between the two modes, with  $PP_{\text{Int}}$  increasing monotonically with current and  $PP_{\text{Bull}}$  showing a strong peak where the bullet forms and then decreasing monotonically towards the noise floor. The different behaviors reflect the different nature of the two modes. While the interior mode expands with current and hence acquires a bigger mode volume covering a larger area of the NC, the self-localized bullet contracts with current and covers a diminishing area of the signal generating region. These pronounced differences suggest that one could also expect qualitatively different behaviors when the two modes are subject to an external signal source at different rf powers ( $P_{rf}$ ).

Figure 3 presents two columns incorporating PSD,  $\Delta f$ , and  $PP$  for interior and bullet modes, respectively, when they are subjected to an external rf source. They are all plotted as a function of half of rf frequency ( $f_{rf}/2$ ). The resulting spectrum is then fitted to a Lorentzian function to extract the power and linewidth. The plots of PSDs versus  $f_{rf}/2$  at  $P_{rf} = -17$  dBm in Figs. 3(a) and 3(b) illustrate how different the two modes are in terms of linewidth, locking bandwidth (BW), and output power. Moreover, in Figs. 3(d) and 3(f), a pronounced parabolic behavior is observed in both bullet  $\Delta f$  and  $PP$ , respectively, which is clearly absent in the interior  $\Delta f$  [Fig. 3(c)] and  $PP$  [Fig. 3(e)]. In addition to this qualitative difference, the maximum  $\Delta f_{\text{Int}}$  is five times lower than  $\Delta f_{\text{Bull}}$  and drops drastically as soon as it locks and reaches the RBW limit of the measurement. However, the bullet mode shows a much more gradual locking which makes the locking BW extraction challenging.

The locking BW is typically extracted by examining the difference between the auto-oscillation frequency and the injected frequency [6,12,33,44]. The locking BW is then defined as the frequency range where the auto-oscillation frequency follows the external injection frequency, or its subharmonics  $f = f_{rf}/2$  in our case. This approach can be

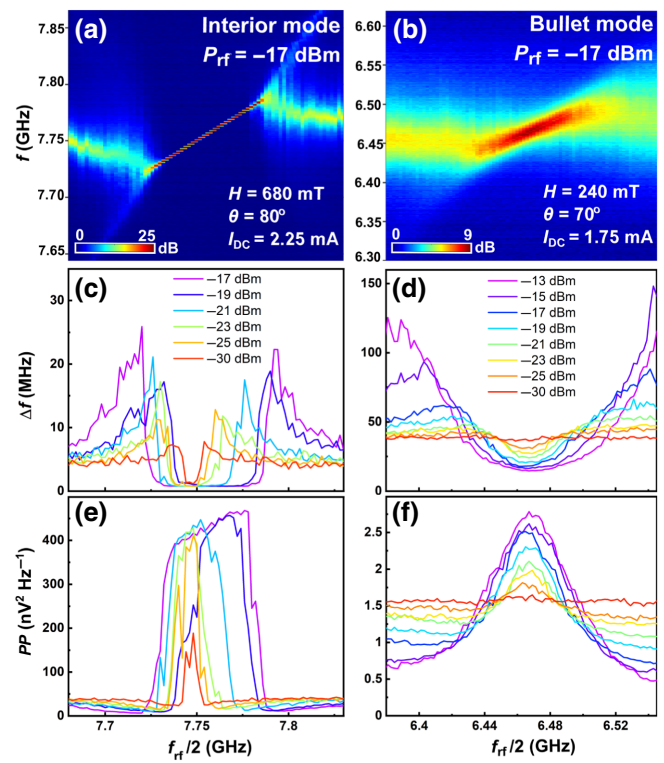


FIG. 3. Power spectral density versus rf frequency of interior (a) and bullet (b) modes, when they are locked to an external rf source at  $P_{rf} = -17$  dBm. Their extracted linewidth, and peak power for interior [bullet] mode at different rf powers are shown in (c) [(d)] and (e) [(f)], respectively.

easily applied to the interior mode [Fig. 3(a)] with a quick and sharp linewidth reduction that counts as a direct indication of locking [45]. However, as shown in Fig. 3(b), the lack of a sharp locking to the external source makes this approach unsuitable for the extraction of the bullet mode injection-locking BW at low power levels where it is difficult to find two accurate locking and releasing points.

In an attempt to define a practical extraction of the locking BW for both modes, we investigate an alternative approach where we plot the frequency difference ( $f - (f_{rf}/2)$ ) as a function of  $f_{rf}/2$ , and extract the zero crossing points of the linear fits to data points with the “largest derivative.” The locking BW is then defined as the distance between the two zero crossing points. The outcome of this approach is shown in Fig. 4(a), where red (blue) circles are the experimental data points for the interior (bullet) mode, and solid black lines define the largest derivative on both sides.

As seen in Fig. 4(a), the interior mode shows sharp locking, meaning that both the “largest derivative” approach and using data points where  $f = f_{rf}/2$  will lead to the same locking BW value. However, this sharp locking and releasing is absent in the bullet mode. We are unable to

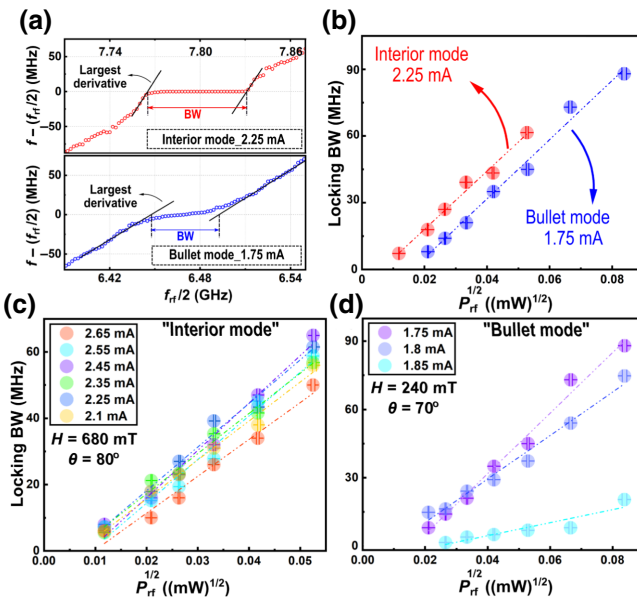


FIG. 4. (a) The BW extraction approach to linearly fit the data points with the largest derivative and extract locking BW. Red (blue) circles are the experimental data points for the interior (bullet) mode, and solid black lines define the largest derivative on both sides ( $P_{rf} = -17$  dBm). (b) A comparative plot of the two modes indicates their difference in power threshold values. Locking BW versus square root of injected power at different drive currents for the (c) interior and (d) bullet mode.

extract the locking BW by the exact matching of oscillator frequency and  $f_{rf}/2$ , since phase slips of the oscillator grow gradually with the detuning frequency. Accordingly, attributing the locking BW to only those points where the oscillator frequency is precisely equal to  $f_{rf}/2$ , will lead to underestimating the locking range, whereas using the largest derivative fitting will lead to a better assessment.

Considering the two PSDs shown in Figs. 3(a) and 3(b) and implementing the extracting approach for both, a comparative plot of the locking BW of two modes is shown in Fig. 4(b). The recorded power spectrum was processed taking into account the gain and losses of the rf circuit from the connecting circuit, cables and the impedance mismatch between the line and the device. Both modes exhibit a square dependency on the injected microwave power (i.e., a linear dependency on the injected microwave current). Moreover, both modes show a power threshold for locking to the external microwave signal. However, this threshold is reduced for the interior mode compared to the bullet mode as seen in Figs. 4(c) and 4(d).

Although employing an identical approach to analyzing the data for both modes lead to reasonable comparison, a quantitative analysis of the injection-locking behavior of the two modes is needed. Hence, we will proceed with a theoretical model which takes the noise level of each mode into account and extracts the corresponding BW values.

#### IV. THEORY FOR INJECTION LOCKING WITH NOISE

To better understand and model the injection locking of the two modes, we employed a theory of oscillator synchronization in the presence of noise [43]. Both oscillation modes in the free-running regime can be fairly well described by a system of coupled equations for the oscillation amplitude and phase, or equivalently by the equation for the complex amplitude  $a$  with a cubic nonlinearity: [46]

$$\frac{da}{dt} + i\omega(p)a + \Gamma_+(p)a - \Gamma_-(p)a = 0, \quad (1)$$

where  $p = |a|^2$ ,  $\omega(p)$  is a power-dependent angular velocity,  $\Gamma_+(p)$  describes natural damping of magnetic oscillations, and  $\Gamma_-(p)$  is the anti-damping contribution from an injected spin current. The operating current sets the amplitude  $A_0$  and frequency  $\omega_0/(2\pi)$  of a free-running oscillator. The nonlinear part of the equation can be described by the following parameters: nonlinear damping  $\Gamma_p = (d\Gamma_+/dp - d\Gamma_-/dp)A_0^2$ , which defines the damping rate of amplitude fluctuations, and frequency nonlinearity  $N = d\omega/dp$ .

The parameters  $N$  and  $\Gamma_p$  are often used through their combination  $\nu = NA_0^2/\Gamma_p$ , that is, the normalized dimensionless frequency shift, which defines the nonisochronous properties of the oscillator and has a strong influence on its behavior, particularly increasing the generation linewidth and locking BW [46,47]. The value of  $\nu$  depends on the applied current [as one can see from the oscillation frequency as a function of the current in Fig. 2(a)] for the following two reasons. First, the amplitude of the magnetization precession grows rapidly with the current, and the cubic term becomes insufficient, so one needs to redefine the nonlinear coefficients as a function of current. Secondly, as mentioned above, the interior mode nucleates at one of the edges of the NC and then shifts toward the center with increasing current, which changes the average demagnetizing field and consequently the nonlinear coefficients. Here we consider the behavior of an oscillator in the vicinity of the operational point on current, where both coefficients are assumed to be constant.

The injection of the rf signal not only shifts the amplitude of the oscillations to the new stationary value  $A_s$ , but also can lead to qualitatively new effects. For example, at high  $P_{rf}$  values, several stable states (e.g., 3 for the cubic nonlinearity) of the oscillator are possible. The transition between these states at the edge of the locking band is reflected in the abrupt jump in the oscillation frequency [48] due to the development of the Hopf bifurcation. Therefore, we assume that the injected rf signal is weak and  $A_s - A_0 \ll A_0$ , which allows us to limit our consideration to an Adler's-like equation for the phase of the

oscillator  $\phi(t)$ :

$$\frac{d\psi}{dt} = 2\pi\Delta - 2\pi\Delta_s \sin\psi + \frac{\xi(t)}{A_0}, \quad (2)$$

where  $\psi(t) = \phi(t) - 2\pi(f_{\text{rf}}/2)t$  is the difference between the phase of the oscillator and rf signal with a frequency  $2(f_{\text{rf}}/2)$  and effective amplitude  $\epsilon_{\text{rf}} \sim P_{\text{rf}}^{1/2}$ ,  $\Delta_s = \epsilon_{\text{rf}}(f_{\text{rf}}/2)/(2A_0)$  is one-sided locking BW in the absence of the noise, and  $\xi(t)$  describes  $\delta$ -like correlated noise  $\langle \xi \xi_\tau \rangle = 2\pi k A_0^2 \delta(\tau)$ , where  $k$  defines the dispersion of the noise, that is, the generation linewidth of the free-running oscillator (half width at half maximum). This approach is at least valid for the analysis of a quasi-isochronous SHNO when  $v \lesssim 1$ . Here, the locking BW  $\Delta_s$  is simply proportional to the amplitude of the rf signal (with the coefficient known as oscillator sensitivity [47]), which is in contrast to the dependence of the extracted BW in Fig. 4, where a clear threshold is observed.

Equation (2) describes the motion of the oscillator phase as a Brownian particle in the periodical inclined potential  $V(\psi)/(2\pi) = -\Delta\psi - \Delta_s \cos\psi$ . The detuning  $\Delta$  defines the potential inclination, while the thermal noise, unlimited in amplitude described by a stochastic term, causes phase jumps (slips) between potential minima. The probabilities and hence the frequencies of slips to the right ( $s_+$ ) and to the left ( $s_-$ ) are different due to inclination, and, knowing the statistical properties of the stochastic process, one can find the forced frequency of the oscillator  $f$  from  $f - (f_{\text{rf}}/2) = \langle d\psi/dt \rangle / 2\pi = s_+ - s_-$ .

For the case of weak noise, when  $2\pi k \ll \Gamma_p$ , it is possible to employ a Fokker-Planck formalism and define the equation for the phase probability density function  $P(\xi, t)$ :

$$\frac{\partial P}{\partial t} + \frac{\partial S}{\partial \psi} = 0, \quad S = s_+ - s_- = -P \frac{dV}{d\psi} - \pi k \frac{\partial P}{\partial \psi}. \quad (3)$$

This method was used in [33] to describe the locking of the SW bullet. The stationary solution  $\bar{P}$  of Eq. (3), when  $\partial P/\partial t = 0$ , leads to the sought-after result, which can be written explicitly following [43]:

$$f - (f_{\text{rf}}/2) = \frac{k}{2\pi} \sinh \frac{2\pi\Delta}{k} |I_{2i\Delta/k}(2\Delta_s/k)|^{-2}, \quad (4)$$

where  $I_{in}(x)$  denotes a Bessel function of the pure imaginary order  $n$ . It should be mentioned that the result of Eq. (4) remains valid for any kind of noise process with a short correlation time (i.e., when  $\tau_{\text{cor}} \ll 1/\Gamma_p$ ) with the replacement of the single coefficient  $k$  by a noise power spectral density  $\kappa(f)$  near the stationary frequency  $k \rightarrow \kappa(f_s) f_s^2 / (2A_0^2)$ .

We can now analyze the behavior of the SHNO locking, using Eq. (4), which has only two parameters, namely the locking BW in the absence of noise,  $\Delta_s$ , and a generation linewidth,  $k$ , of the free-running oscillator.

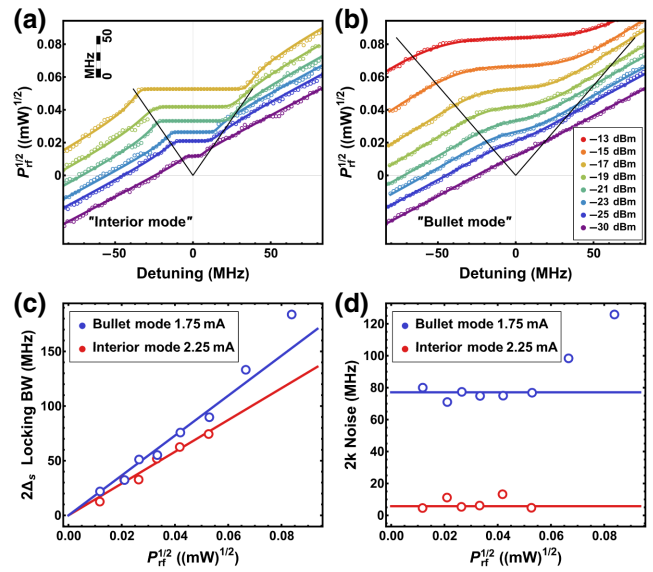


FIG. 5. Forced frequency  $f - (f_{\text{rf}}/2)$  of (a) linear and (b) bullet mode as a function of detuning  $\Delta$ . Circles show the experimental data, while solid lines show fits according to Eq. (4). The offset between the plots corresponds to the amplitude of the applied rf signal, shown on the  $y$  axis. The frequency scale is shown in the inset. Solid black lines show the extracted value of the locking bandwidth  $\Delta_s$ , forming Arnold's tongues. (c) Locking bandwidth  $2\Delta_s$ , extracted from the fit versus applied rf amplitude. (d) Noise parameter  $2k$  extracted from the fitting, versus applied rf amplitude. Solid lines show median values.

The experimental data were fitted by Eq. (4) and the extracted parameters  $\Delta_s$  and  $k$  are shown in Fig. 5. As expected, the  $\Delta_s$  is proportional to the applied rf amplitude. More prominent are the similar values of the slopes, that is, the SHNO's sensitivities for the bullet and interior modes which have also been seen from fitting in Fig. 4(b). Thus, all the differences in the observed locking behavior between bullet and linear modes are due to the drastically different noise values. When  $k > \Delta_s$  (i.e., at low applied rf powers), the phase of the oscillator can easily jump between minima of the potential  $V$  and the locking is absent. This creates a threshold in the experimentally observed locking BW, as discussed for the bullet mode in [33]. Indeed, the visible frequency pulling of the bullet mode by rf signal can be observed at  $P_{\text{rf}} \geq -23$  dBm [Fig. 5(b)], where already  $\Delta_s > k$  [Fig. 5(c)].

With an increase in the detuning frequency  $\Delta$  the potential  $V$  inclines, leading to a reduction of the height of a potential barrier between minima. In the noiseless case, the edge of the locking band corresponds to vanishing barrier, while in the presence of noise the locking is broken at the lower detunings  $\Delta$ , when the height of the potential barrier becomes comparable to the thermal energy. Thus, the experimentally observable locking BW (Fig. 4) is always lower than  $\Delta_s$ .

As one can see from Fig. 5(d), the noise values obtained for high rf amplitudes ( $-15$  dBm and  $-13$  dBm) lie well above the median value. The most obvious explanation is the thermal heating of the sample by rf injection and the developing of the bifurcation, described earlier. Therefore, we speculate that at  $P_{\text{rf}} = -15$  dBm the applied signal cannot be considered as weak, which defines the limit of the applicability of the theory for the given SHNO.

## V. CONCLUSION

We have studied the injection-locking behavior of two distinctly different SW modes in a single SHNO when subjected to injection locking to an external rf signal at twice its frequency. We initially excited a self-localized SW bullet soliton and an extended interior mode in a single SHNO by varying the oblique magnetic field angle and magnitude, followed by injection locking to an external microwave signal. Experimental observation reveals two qualitatively different responses to injection locking in terms of linewidth, output power, and locking BW. We extract their locking BW by defining a “unified” approach based on the data points with the largest derivative, which leads to observing an apparent threshold in external power before a successful locking. However, employing a theory of oscillator synchronization in the presence of noise confirms the absence of a threshold when the noise is absent. Consequently, the very different locking behaviors of the two modes and the observation of a threshold stem from the different intrinsic noise levels of the modes which exceed an order-of-magnitude difference. Our work highlights that a complete model, including noise level, must be used for the oscillators with higher noise levels, for example, for the SW bullet investigated in this work.

The data that support the findings of this study are available from the corresponding author upon reasonable request.

## ACKNOWLEDGMENTS

This work was supported by the Swedish Research Council (VR) and the Horizon 2020 research and innovation programme (ERC Advanced Grant No. 835068 “TOPSPIN”).

- [1] R. Adler, A study of locking phenomena in oscillators, *Proc. IRE* **34**, 351 (1946).
- [2] T. Chen, R. K. Dumas, A. Eklund, P. K. Muduli, A. Houshang, A. A. Awad, Dürrenfeld, B. G. Malm, A. Rusu, and J. Åkerman, Spin-torque and spin-Hall nano-oscillators, *Proc. IEEE* **104**, 1919 (2016).
- [3] W. H. Rippard, M. R. Pufall, S. Kaka, T. J. Silva, S. E. Russek, and J. A. Katine, Injection Locking and Phase Control of Spin Transfer Nano-oscillators, *Phys. Rev. Lett.* **95**, 067203 (2005).

- [4] Y. Zhou, J. Persson, and J. Åkerman, Intrinsic phase shift between a spin torque oscillator and an alternating current, *J. Appl. Phys.* **101**, 09A510 (2007).
- [5] Y. Zhou, J. Persson, S. Bonetti, and J. Åkerman, Tunable intrinsic phase of a spin torque oscillator, *Appl. Phys. Lett.* **92**, 092505 (2008).
- [6] B. Georges, J. Grollier, M. Darques, V. Cros, C. Deranlot, B. Marcilhac, G. Faini, and A. Fert, Coupling Efficiency for Phase Locking of a Spin Transfer Nano-oscillator to a Microwave Current, *Phys. Rev. Lett.* **101**, 017201 (2008).
- [7] M. Romera, P. Talatchian, R. Lebrun, K. J. Merazzo, P. Bortolotti, L. Vila, J. D. Costa, R. Ferreira, P. P. Freitas, M.-C. Cyrille, U. Ebels, V. Cros, and J. Grollier, Enhancing the injection locking range of spin torque oscillators through mutual coupling, *Appl. Phys. Lett.* **109**, 252404 (2016).
- [8] Emilie Jué, Matthew R. Pufall, and William H. Rippard, Asymmetric and partial injection locking of a three-terminal spin-torque oscillator, *Appl. Phys. Lett.* **112**, 102403 (2018).
- [9] M. Tortarolo, B. Lacoste, J. Hem, C. Dieudonné, M. C. Cyrille, J. A. Katine, D. Mauri, A. Zeltser, L. D. Buda-Prejbeanu, and U. Ebels, Injection locking at 2f of spin torque oscillators under influence of thermal noise, *Sci. Rep.* **8**, 1 (2018).
- [10] J. Hem, L. D. Buda-Prejbeanu, and U. Ebels, Power and phase dynamics of injection-locked spin torque nano-oscillators under conservative and dissipative driving signals, *Phys. Rev. B* **100**, 054414 (2019).
- [11] Jérémie Létang, Sébastien Petit-Watelot, Myoung-Woo Yoo, Thibaut Devolder, Karim Bouzehouane, Vincent Cros, and Joo-Von Kim, Modulation and phase-locking in nanocontact vortex oscillators, *Phys. Rev. B* **100**, 144414 (2019).
- [12] T. Hache, T. Weinhold, K. Schultheiss, J. Stigloher, F. Vilsmeier, C. Back, S. S. P. K. Arekapudi, O. Hellwig, J. Fassbender, and H. Schultheiss, Combined frequency and time domain measurements on injection-locked, constriction-based spin Hall nano-oscillators, *Appl. Phys. Lett.* **114**, 102403 (2019).
- [13] Sergei Urazhdin, Phillip Tabor, Vasil Tiberkevich, and Andrei Slavin, Fractional Synchronization of Spin-Torque Nano-oscillators, *Phys. Rev. Lett.* **105**, 104101 (2010).
- [14] Phillip Tabor, Vasil Tiberkevich, Andrei Slavin, and Sergei Urazhdin, Hysteretic synchronization of nonlinear spin-torque oscillators, *Phys. Rev. B* **82**, 020407 (2010).
- [15] S. Perna, L. Lopez-Diaz, M. D’Aquino, and C. Serpico, Large hysteresis effect in synchronization of nanocontact vortex oscillators by microwave fields, *Sci. Rep.* **6**, 1 (2016).
- [16] Hanuman Singh, K. Konishi, S. Bhuktare, A. Bose, S. Miwa, A. Fukushima, K. Yakushiji, S. Yuasa, H. Kubota, Y. Suzuki, and A. A. Tulapurkar, Integer, Fractional, and Sideband Injection Locking of a Spintronic Feedback Nano-oscillator to a Microwave Signal, *Phys. Rev. Appl.* **8**, 064011 (2017).
- [17] Hanuman Singh, A. Bose, S. Bhuktare, A. Fukushima, K. Yakushiji, S. Yuasa, H. Kubota, and Ashwin A. Tulapurkar, Self-injection locking of a spin torque nano-oscillator to magnetic field feedback, *Phys. Rev. Appl.* **10**, 024001 (2018).

- [18] Yi Li, Xavier de Milly, Flavio Abreu Araujo, Olivier Klein, Vincent Cros, Julie Grollier, and Grégoire de Loubens, Probing Phase Coupling between Two Spin-Torque Nano-oscillators with an External Source, *Phys. Rev. Lett.* **118**, 247202 (2017).
- [19] A. Litvinenko, P. Sethi, C. Murapaka, A. Jenkins, V. Cros, P. Bortolotti, R. Ferreira, B. Dieny, and U. Ebels, Analog and Digital Phase Modulation and Signal Transmission with Spin-Torque Nano-oscillators, *Phys. Rev. Appl.* **16**, 024048 (2021).
- [20] Lang Zeng, Yang Liu, Hao-Hsuan Chen, Yan Zhou, Deming Zhang, Youguang Zhang, and Weisheng Zhao, Robust phase shift keying modulation method for spin torque nano-oscillator, *Nanotechnology* **31**, 375205 (2020).
- [21] K. Yogendra, D. Fan, B. Jung, and K. Roy, Magnetic pattern recognition using injection-locked spin-torque nano-oscillators, *IEEE Trans. Electron Devices* **63**, 1674 (2016).
- [22] Miguel Romera, Philippe Talatchian, Sumito Tsunegi, Flavio Abreu Araujo, Vincent Cros, Paolo Bortolotti, Juan Trastoy, Kay Yakushiji, Akio Fukushima, Hitoshi Kubota, Shinji Yuasa, Maxence Ernoult, Damir Vodenicarevic, Tifenn Hirtzlin, Nicolas Locatelli, Damien Querlioz, and Julie Grollier, Vowel recognition with four coupled spin-torque nano-oscillators, *Nature* **563**, 230 (2018).
- [23] Mohammad Zahedinejad, Ahmad A. Awad, Shreyas Muralidhar, Roman Khymyn, Himanshu Fulara, Hamid Mazraati, Mykola Dvornik, and Johan Åkerman, Two-dimensional mutually synchronized spin Hall nano-oscillator arrays for neuromorphic computing, *Nat. Nanotechnol.* **15**, 47 (2020).
- [24] Brooke C. McGoldrick, Jonathan Z. Sun, and Luqiao Liu, Ising Machine Based on Electrically Coupled Spin Hall Nano-oscillators, *Phys. Rev. Appl.* **17**, 014006 (2022).
- [25] Giovanni Finocchio *et al.*, Roadmap for unconventional computing with nanotechnology, (2023), 10.48550/arXiv.2301.06727.
- [26] A. V. Chumak *et al.*, Advances in magnetics roadmap on spin-wave computing, *IEEE Trans. Magn.* **58**, 1 (2022).
- [27] V. E. Demidov, S. Urazhdin, A. Zholud, A. V. Sadovnikov, and S. O. Demokritov, Nanoconstriction-based spin-Hall nano-oscillator, *Appl. Phys. Lett.* **105**, 172410 (2014).
- [28] A. A. Awad, P. Dürrenfeld, A. Houshang, M. Dvornik, E. Iacocca, R. K. Dumas, and J. Åkerman, Long-range mutual synchronization of spin Hall nano-oscillators, *Nat. Phys.* **13**, 292 (2017).
- [29] Akash Kumar, Himanshu Fulara, Roman Khymyn, Mohammad Zahedinejad, Mona Rajabali, Xiaotian Zhao, Nilamani Behera, Afshin Houshang, Ahmad A. Awad, and Johan Åkerman, Robust mutual synchronization in long spin hall nano-oscillator chains (2023).
- [30] Ahmad A. Awad, Afshin Houshang, Mohammad Zahedinejad, Roman Khymyn, and Johan Åkerman, Width dependent auto-oscillating properties of constriction based spin Hall nano-oscillators, *Appl. Phys. Lett.* **116**, 232401 (2020).
- [31] M. Zahedinejad, H. Mazraati, H. Fulara, J. Yue, S. Jiang, A. A. Awad, and J. Åkerman, CMOS compatible W/CoFeB/MgO spin Hall nano-oscillators with wide frequency tunability, *Appl. Phys. Lett.* **112**, 1 (2018).
- [32] Mohammad Zahedinejad, Ahmad A. Awad, Philipp Dürrenfeld, Afshin Houshang, Yuli Yin, Pranaba K. Muduli, and Johan Åkerman, Current modulation of nanoconstriction spin-Hall nano-oscillators, *IEEE Magn. Lett.* **8**, 1 (2017).
- [33] V. E. Demidov, H. Ulrichs, S. V. Gurevich, S. O. Demokritov, V. S. Tiberkevich, A. N. Slavin, A. Zholud, and S. Urazhdin, Synchronization of spin Hall nano-oscillators to external microwave signals, *Nat. Commun.* **5**, 3179 (2014).
- [34] A. Slavin and V. Tiberkevich, Spin Wave Mode Excited by Spin-Polarized Current in a Magnetic Nanocontact is a Standing Self-Localized Wave Bullet, *Phys. Rev. Lett.* **95**, 237201 (2005).
- [35] S. Bonetti, V. Tiberkevich, G. Consolo, G. Finocchio, P. Muduli, F. Mancoff, A. Slavin, and J. Åkerman, Experimental Evidence of Self-Localized and Propagating Spin Wave Modes in Obliquely Magnetized Current-Driven Nanocontacts, *Phys. Rev. Lett.* **105**, 217204 (2010).
- [36] M. Dvornik, A. A. Awad, and J. Åkerman, Origin of Magnetization Auto-oscillations in Constriction-Based Spin Hall Nano-oscillators, *Phys. Rev. Appl.* **9**, 014017 (2018).
- [37] Zheng Duan, Andrew Smith, Liu Yang, Brian Youngblood, Jürgen Lindner, Vladislav E. Demidov, Sergej O. Demokritov, and Ilya N. Krivorotov, Nanowire spin torque oscillator driven by spin orbit torques, *Nat. Commun.* **5**, 5616 (2014).
- [38] Hamid Mazraati, Seyyed Ruhollah Etesami, Seyed Amir Hossein Banuazizi, Sunjae Chung, Afshin Houshang, Ahmad A. Awad, Mykola Dvornik, and Johan Åkerman, Auto-oscillating Spin-Wave Modes of Constriction-Based Spin Hall Nano-oscillators in Weak In-plane Fields, *Phys. Rev. Appl.* **10**, 054017 (2018).
- [39] Philipp Dürrenfeld, Ahmad A. Awad, Afshin Houshang, Randy K. Dumas, and Johan Åkerman, A 20 nm spin Hall nano-oscillator, *Nanoscale* **9**, 1285 (2017).
- [40] B. Divinskiy, S. Urazhdin, V. E. Demidov, A. Kozhanov, A. P. Nosov, A. B. Rinkevich, and S. O. Demokritov, Magnetic droplet solitons generated by pure spin currents, *Phys. Rev. B* **96**, 224419 (2017).
- [41] H. Fulara, M. Zahedinejad, R. Khymyn, A. A. Awad, S. Muralidhar, M. Dvornik, and J. Åkerman, Spin-orbit torque–driven propagating spin waves, *Sci. Adv.* **5**, 1 (2019).
- [42] Boris Divinskiy, Vladislav E. Demidov, Sergei Urazhdin, Ryan Freeman, Anatoly B. Rinkevich, and Sergej O. Demokritov, Excitation and amplification of spin waves by spin–orbit torque, *Adv. Mater.* **30**, 1802837 (2018).
- [43] Rouslan L. Stratonovich, *Topics in the Theory of Random Noise* (Gordon and Breach, New York, 1967), Vol. 2.
- [44] Naveen Sisodia and P. K. Muduli, Simultaneous enhancement of spin-torque diode sensitivity and frequency by voltage controlled magnetic anisotropy and parametric synchronization, *Appl. Phys. Lett.* **115**, 102401 (2019).
- [45] William Rippard, Matthew Pufall, and Anthony Kos, Time required to injection-lock spin torque nanoscale oscillators, *Appl. Phys. Lett.* **103**, 182403 (2013).
- [46] A. Slavin and V. Tiberkevich, Nonlinear auto-oscillator theory of microwave generation by spin-polarized current, *IEEE Trans. Magn.* **45**, 1875 (2009).
- [47] Vasil S. Tiberkevich, Roman S. Khymyn, Hong X. Tang, and Andrei N. Slavin, Sensitivity to external signals and synchronization properties of a non-isochronous auto-oscillator with delayed feedback, *Sci. Rep.* **4**, 1 (2014).
- [48] Arkady Pikovsky, Michael Rosenblum, and Jürgen Kurths, Phase synchronization in regular and chaotic systems, *Int. J. Bifurcation Chaos* **10**, 2291 (2000).